

# X-ray interferometer with narrow beam

V. L. Indenbom, I. Sh. Slobodetskii, and K. G. Truni

Crystallography Institute, USSR Academy of Sciences  
Institute of High-Pressure Physics, USSR Academy of Sciences  
(Submitted September 25, 1973)

Zh. Eksp. Teor. Fiz. 66, 1110-1120 (March 1974)

The wave field produced as a result of successive diffraction of a spatially inhomogeneous beam of x-rays in two equally oriented crystals is investigated. The theory developed explains the interference phenomena that occur in split beams without their superposition, and predicts the feasibility of using two-crystal x-ray interferometers as high-resolution diffraction lenses that may be useful in x-ray spectroscopy, defectoscopy, and interferometry.

The existing theory of x-ray interferometers deals with interference phenomena produced by superposition of previously split broad beams of x rays, and serves as the basis of practical applications of interferometers for the determination of the refractive indices of substances, for precision measurements of differences between lattice orientations and parameters of crystal glass, and for analysis of small crystal distortions by means of moire patterns. From experiments with narrow beams it is known, however, that an interference pattern can be produced in each individual beam without superimposing the beams one on the other [1-3]. The interpretation of these patterns calls for the investigation of the diffraction of spatially-inhomogeneous beams and cannot be obtained within the framework of the usual plane- or spherical-wave approximations.

In this article we consider the principal laws governing the formation of an x-ray wave field in the case of successive diffraction of a bounded x-ray beam in the crystal blocks of an interferometer. We investigate the conditions for both diffraction spreading and diffraction sharpening (focusing) of wave packets, up to a practical reconstruction of the initial shape of the packet. The developed theory explains the interference effects observed previously in experiments and points to the possibility of development of new trends in x-ray interferometry, spectroscopy, and flaw detection.

## 1. FORMULATION OF PROBLEM

We consider the simplest variant of a two-crystal interferometer (Fig. 1). The plates of the interferometer are parallel to one another and are cut in such a way that the reflecting planes  $x = \text{const}$  are perpendicular to the surfaces of the plates  $z = \text{const}$  (Laue-Laue type interferometer). The first plates split the incident x-ray beam into a transmitted beam  $E_0$  and a reflected beam  $E_1$ . Past the second plate we have four beams: 1) the beam  $E_{00}$  which is transmitted in both plates; 2) the beam  $E_{10}$ , transmitted in the first plate and reflected in the second; 3) the beam  $E_{01}$ , reflected in both plates (with direct and inverse diffraction vector); 4) the beam  $E_{11}$  reflected in the first plate and transmitted in the second.

The amplitudes  $E_0(x)$  and  $E_1(x)$  of the wave fields making up the transmitted and reflected waves are connected in each plate by the influence functions  $G_{ij}(x-x', z-z')$ , which determine the influence of the field  $E_j$  at the point  $(x', z')$  of the scattering plane on the field  $E_i$  at the point  $(x, z)$  of the same plane [4]:

$$E_i(x, z) = \int G_{ij}(x-x', z-z') E_j(x', z') dx', \quad (1)$$

where the integration is carried out over the section

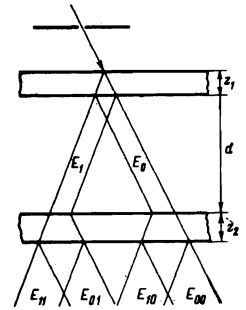


FIG. 1. Beam splitting in two-crystal interferometer of the Laue-Laue type.

$z' = \text{const}$  of the scattering plane. With the aid of the Riemann function

$$G(x, z) = \frac{1}{2} J_0 \left( \frac{\chi}{2} \sqrt{z^2 - x^2} \right) \exp \left[ -\frac{i\alpha_0}{4} (z-x) \right] \Theta(z-|x|) \quad (2)$$

of the telegrapher's equation with constant coefficients, describing the propagation of an x-ray wave field in a crystal, the influence functions are given by the following expressions

$$\begin{aligned} G_{00}(x, z) &= \left( \frac{i\alpha}{2} + \frac{\partial}{\partial z} - \frac{\partial}{\partial x} \right) G(x, z), \\ G_{10}(x, z) &= \frac{i\chi_1 C}{2} G(x, z), \\ G_{01}(x, z) &= \frac{i\chi_{-1} C}{2} G(x, z), \\ G_{11}(x, z) &= \left( \frac{\partial}{\partial z} + \frac{\partial}{\partial x} \right) G(x, z). \end{aligned} \quad (3)$$

Here  $J_0(z)$  is a Bessel function of zero order,  $\Theta(x) = 0$  at  $x < 0$  and  $\Theta(x) = 1$  at  $x > 0$ ;  $\chi_1$  and  $\chi_{-1}$  are the Fourier components of the polarizability of the crystal for the wave vector coinciding with the diffraction vector and the inverse to it;  $C$  is the polarization factor:  $C = 1$  for the wave-field components polarized in the scattering plane and  $C = \cos 2\theta$ , where  $\theta$  is the Bragg angle, for the components polarized perpendicular to this plane;  $\chi = \sqrt{\chi_1 \chi_{-1} C}$ ; the parameter  $\alpha$  characterizes the deviation of the crystal from the exact Bragg orientation. We choose the standard dimensionless coordinate system [4], in which the  $x$  axis is antiparallel to the diffraction vector, the  $z$  axis is parallel to the transmission direction, and the propagation directions of the transmitted and reflected waves make an angle of  $90^\circ$ .

If a narrow beam of unit intensity, i.e.,  $E_0(x, 0) = \delta(x)$  and  $E_1(x, 0) = 0$ , is incident on the surface  $z = 0$  of the first plate, then the wave field in the first plate is given directly by the influence functions (3). On the exit surface of the first plate ( $z = z_1$ ) we have

$$E_0(x, z_1) = G_{00}(x, z_1), \quad E_1(x, z_1) = G_{10}(x, z_1). \quad (4)$$

After passing through an air gap of length  $d$ , the wave

packets (4) are incident on the entrance face  $z = z_1 + d$  of the second plate, with a shift  $\pm d$ :

$$E_0(x, z_1 + d) = G_{00}(x - d, z_1), \quad E_1(x, z_1 + d) = G_{10}(x + d, z_1). \quad (5)$$

The wave field in the second plate is given by convolutions, of the type (1), of the fields (5) with the influence functions (3). After passing through the second plate of thickness  $z_2$  we have four beams:

$$E_{00}(x, z_1 + z_2 + d) = \int G_{00}(z_2, x - x') G_{00}(x' - d, z_1) dx', \quad (6)$$

$$E_{10}(x, z_1 + z_2 + d) = \int G_{10}(z_2, x - x') G_{00}(x' - d, z_1) dx', \quad (7)$$

$$E_{01}(x, z_1 + z_2 + d) = \int G_{01}(z_2, x - x') G_{10}(x' + d, z_1) dx', \quad (8)$$

$$E_{11}(x, z_1 + z_2 + d) = \int G_{11}(z_2, x - x') G_{10}(x' + d, z_1) dx'. \quad (9)$$

The problem reduces thus to a calculation of the convolutions  $G_{00} * G_{00}$ ,  $G_{10} * G_{00}$ ,  $G_{01} * G_{10}$  and  $G_{11} * G_{10}$ . We note that at  $d = 0$  the interferometer plates are in contact and the wave fields  $E_0 = E_{00} + E_{01}$  and  $E_1 = E_{10} + E_{11}$  on the exit surface of the crystal are given by the well-known influence functions  $G_{00}$  and  $G_{10}$ , i.e.,

$$G_{00}(x, z_2) * G_{00}(x, z_1) + G_{01}(x, z_2) * G_{10}(x, z_1) = G_{00}(x, Z), \quad (10)$$

$$G_{10}(x, z_2) * G_{00}(x, z_1) + G_{11}(x, z_2) * G_{10}(x, z_1) = G_{10}(x, Z), \quad (11)$$

where the right-hand sides contain the usual influence functions for a plate with total thickness  $Z = z_1 + z_2$ .

Taking (10), (11), and the relations (3) into account, we can express all the sought convolutions in terms of the convolution (8), which determines the field of the doubly-refracted wave  $E_{01}$ .

## 2. DISTRIBUTION OF THE AMPLITUDES IN A DOUBLY-REFRACTED WAVE

The calculation of the convolution (8) is of greatest interest, since it is the doubly-refracted beam  $E_{01}$  which is usually investigated in experiment. Using the Fourier representation of the Riemann function (2)

$$G(x) = \frac{1}{2\pi} \int_{-\infty}^{\infty} d\omega e^{i\omega x} \frac{\sin \Omega x}{\Omega} \exp\left[-\frac{i\alpha}{4}(z-x)\right], \quad \Omega = \sqrt{\omega^2 + \chi^2/4}, \quad (12)$$

we can reduce the convolution (8) to a convolution of the Fourier components of the Riemann function:

$$\begin{aligned} G_{01} * G_{10} &= \int_{-\infty}^{\infty} G_{01}(x-x', z_2) G_{10}(x', z_1) dx' = -\frac{\chi^2}{16} \int_{-\infty}^{\infty} G(x-x', z_2) G(x', z_1) dx' \\ &= -\frac{\chi^2}{4} \exp\left[-\frac{i\alpha}{4}(Z-x)\right] I(x, z_1, z_2), \end{aligned} \quad (13)$$

where

$$I(x, z_1, z_2) = \frac{2}{\pi} \int_{-\infty}^{\infty} d\omega e^{i\omega x} \frac{\sin \Omega z_1 \sin \Omega z_2}{\Omega^2}. \quad (14)$$

We consider the derivative

$$\begin{aligned} \frac{\partial I}{\partial z_1} &= \frac{1}{\pi} \int_{-\infty}^{\infty} d\omega e^{i\omega x} \frac{\sin \Omega Z + \sin \Omega \delta}{\Omega} = J_0\left(\frac{\chi}{2} \sqrt{Z^2 - x^2}\right) \Theta(Z - |x|) \\ &+ \text{sign } \delta J_0\left(\frac{\chi}{2} \sqrt{\delta^2 - x^2}\right) \Theta(|\delta| - |x|), \end{aligned} \quad (15)$$

where  $\delta = z_2 - z_1$ . Integration of (15) with respect to the variable  $z_1$  with allowance for the initial condition  $I(x, 0, z_2) = 0$  and of the symmetry of the function  $I(x, z_1, z_2)$  with respect to the variables  $z_1$  and  $z_2$  yield, after substituting in (13)

$$G_{01} * G_{10} = -\frac{\chi^2}{16} \exp\left[-\frac{i\alpha}{4}(Z-x)\right] \int_{\max(|x|, |\delta|)}^Z J_0\left(\frac{\chi}{2} \sqrt{t^2 - x^2}\right) dt \Theta(Z - |x|). \quad (16)$$

It follows from (16) that the amplitude of the wave

field  $E_{01}$  as a function of the variables  $\delta$  and  $x$  on the boundary  $|\delta| = |x|$  remains continuous, but experience a discontinuity of the slope, and in the case of an interferometer with wedge-shaped plates this discontinuity should correspond to kinks in the interference lines.

## 3. THE PARTICULAR CASE $z_1 = z_2$ . X-RAY DIFFRACTION LENS

At  $z_1 = z_2$ , the convolution (16) takes the simple form

$$G_{01} * G_{10} = -\frac{\chi^2}{16} \exp\left[-\frac{i\alpha}{4}(Z-x)\right] \Theta(Z - |x|) \int_{|x|}^Z J_0\left(\frac{\chi}{2} \sqrt{t^2 - x^2}\right) dt. \quad (17)$$

At the center of the beam the amplitude of the wave fields reaches a maximum where height and shape can be estimated by using the tabulated integral

$$\int_x^{\infty} J_0\left(\frac{\chi}{2} \sqrt{t^2 - x^2}\right) dt = \frac{2}{\chi} e^{-\chi x/2} \quad (x > 0), \quad (18)$$

from which it follows for  $\chi Z \gg 1$  and  $|x| \ll Z$  that

$$G_{01} * G_{10} \approx -\frac{\chi}{8} \exp\left[-\frac{i\alpha}{4}(Z-x) - \frac{\chi}{2}|x|\right]. \quad (19)$$

with respect to the extinction length  $\Lambda = 2\pi/\chi$ , the half-width of the intensity peak of the image is  $\Lambda/2\pi$  (when changing over to absolute units, this quantity should be multiplied by  $\tan \theta$ ).

When  $|x|$  approaches  $Z$ , we have

$$\begin{aligned} \int_{|x|}^Z J_0\left(\frac{\chi}{2} \sqrt{t^2 - x^2}\right) dt &= \int_0^{\sqrt{Z^2 - x^2}} J_0\left(\frac{\chi}{2} t\right) \frac{t dt}{\sqrt{t^2 + x^2}} \\ &\approx \frac{1}{|x|} \int_0^{\sqrt{Z^2 - x^2}} J_0\left(\frac{\chi}{2} t\right) t dt = \frac{2}{\chi|x|} \sqrt{Z^2 - x^2} J_1\left(\frac{\chi}{2} \sqrt{Z^2 - x^2}\right). \end{aligned} \quad (20)$$

As a result, the wave field near the edges of the beam oscillates with an amplitude which is approximately  $\chi Z/2$  times smaller than the amplitude of the central peak (19), and vanishes on the boundary characteristics  $|x| = Z$ .

By way of example, Fig. 2 shows the intensity distribution of the field  $E_{01}$  for  $\chi Z = 80$ . This corresponds, e.g., to the reflection of  $\text{MoK}\alpha$  radiation from the (220) plane of silicon ( $\Lambda \approx 35 \mu$ ,  $\theta \approx 10.6^\circ$ ) in an interferometer with plates of approximate thickness 0.45 mm. Since the height of the peak in Fig. 2 exceeds the background intensity by two orders of magnitude, and the half-width of the peak  $\Lambda \tan \theta/2\pi$  is of the order of a micron, the interferometer serves in this case as an x-ray diffraction lens: the first plate produces a broad diffraction image of the slit, while the second plate again gathers the diffracted x-rays into a narrow beam, the rays with different polarizations being gathered into one and the same place. By replacing the slit on the entrance surface of the interferometer by a screen with holes, by a semitransparent plate, or by a figure, we obtain in the  $E_{01}$  beam full-size high-accuracy x-ray images of these objects.

It should be noted that at  $z_2 > z_1$  the diffraction focusing of the beam  $E_{01}$  in the second plate occurs at a depth  $z_1$  from its entrance surface. This effect can apparently be used to investigate dislocations or other crystal defects located at a given depth. The focusing effect is illustrated in Fig. 3 by the calculated pattern of the distribution of the wave-field intensity in the scattering plane in both plates of the interferometer. The wave field  $E_1$  in the first plate (Fig. 3a) is described by the

influence function  $G_{10}$ . The interference fringes take the form of hyperbolas  $z^2 - x^2 = \text{const}$ . In the wave field  $E_{01}$  in the second plate (Fig. 3b) one can clearly see at  $|x| < |\delta|$  interference fringes with the concave sides towards the focus  $x = \delta = 0$ . In the region  $|x| > |\delta|$  one

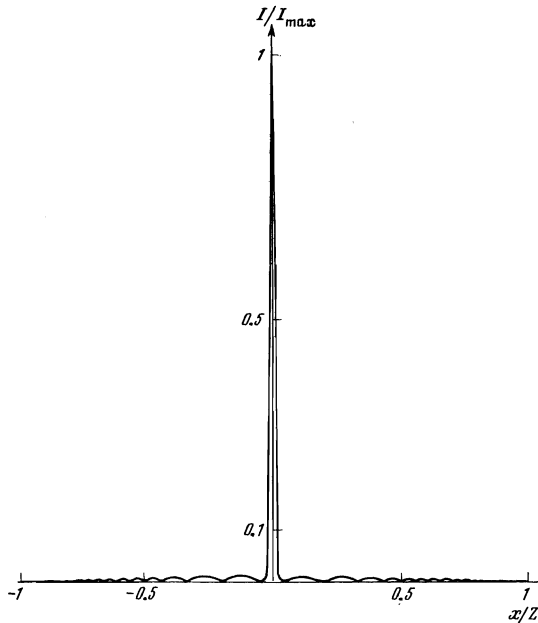


FIG. 2. Effect of diffraction focusing of a doubly refracted beam. It is assumed that  $z_1 = z_2$ ,  $\alpha = 0$ , and  $\chi z = 80$ .

observes relatively weak interference fringes similar to the interference fringes in the first plate. Figure 2 corresponds to a section through Fig. 3 at the level of the "focus."

#### 4. THE DIFFRACTION LENS AS A SPECTROMETER

By way of another example of the use of the focusing effect we can point to the problem of spectral resolution of x rays<sup>[5]</sup>. In this case the spectrometer is very compact, because of the focusing of the image of each line of the spectrum, and requires no adjustment. If the distance from the slit to the recording photographic plate, less the thickness of the plates, amounts to  $D$ , then a change  $\delta\lambda$  in the radiation wavelength changes the coordinate  $x = D \tan \theta$  of the line by an amount

$$\delta x = \frac{D \tan \theta}{\lambda} \delta\lambda (1 + \tan^2 \theta). \quad (21)$$

At  $D \sim 3$  cm,  $\tan \theta \sim 0.2$ ,  $\lambda \sim 0.5 \text{ \AA}$ , and a line width  $\delta x \sim 10^{-4}$  cm, the resolution of a diffraction-lens spectrometer is approximately  $10^{-4} \text{ \AA}$ . This sensitivity suffices to solve many problems of x-ray spectrum analysis. It is possible to solve in similar fashion a problem typical of x-ray microanalysis, namely that of obtaining a monochromatic x-ray image of a sample.

#### 5. THEORY OF THE "IMAGE INVERSION" EFFECT

Formulas (13)–(16) provide a simple explanation of the experimentally observed inversion of the interference pattern in an interferometer with a tapered crystal.

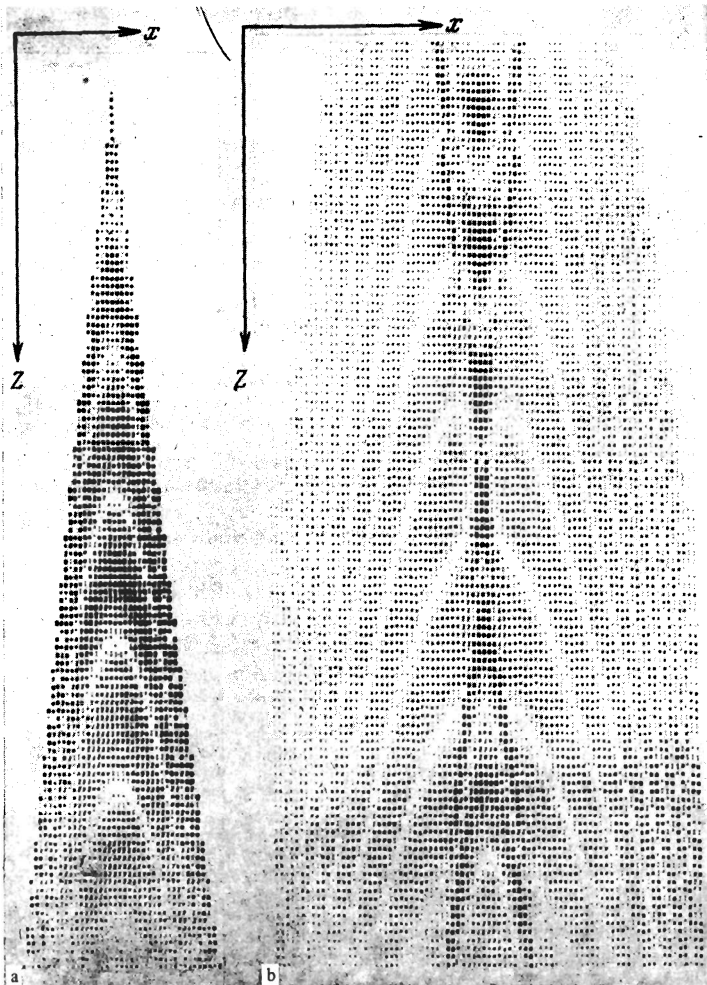


FIG. 3. Computer-calculated distribution of the intensity of the wave field  $E_1$  (a) and of the wave field  $E_{01}$  (b) in the scattering plane.

As is well known, the wedge produces in the reflected wave a narrow-slit image of the type (4), with interference fringes in the form of hyperbolas  $z^2 - x^2 = \text{const}$ . The order of the interference, naturally, increases from the peak to the base of the wedge. On the whole, the picture of the fringes is similar to that shown in Fig. 3a, if the coordinate  $z$  is taken to mean the distance from the scattering plane to the vertex of the wedge. As first observed by Hart and Milne<sup>[3]</sup>, in an interferometer with a tapered plate, the slit image is radically altered past the second plate: in the central part of the image the curvature of the fringes reverses sign, and the picture as a whole experiences as it were an inversion. The customary image inversion of optical lenses is impossible here, however, inasmuch as the diffraction phenomena occur independently in each scattering plane (corresponding to a horizontal section through Fig. 3a).

The seeming inversion of the image can be easily explained if it is recognized that, according to (16), the slit image produced by the thin part of the wedge ( $z_1 \ll z_2$ ), and containing a small number of interference fringes, acquires a large number of fringes after diffraction in the second plate of the interferometer, while the image produced by the thick part of the wedge ( $z_1 \sim z_2$ ) and containing many fringes contracts into a narrower image that is less rich in fringes. In the limiting case  $z_1 = z_2$  we obtain the extremely narrow image (19).

By way of illustration, Fig. 4 shows the interference pattern produced in the beam  $E_{01}$  at the exit of an interferometer in which the second plate has a thickness equal to the thickness of the base of the first tapered plate. In the region  $|x| < |\delta|$  in comparison with the slit image in the first plate (Fig. 3a), the order of the interference is reversed, the interference fringes are bent in the opposite direction, and are turned with their vertices to the "focus"  $x = \delta = 0$ . On the boundary  $|x| = |\delta|$ , kinks appear on the contours of equal image intensity. In the region  $|x| > |\delta|$  one observes only weak interference fringes that are bent similar to those in Fig. 3a. It is interesting to note that an investigation of our problem in the geometrical-optics approximation<sup>[2]</sup> yields in place of (16) a sum of diverging and converging cylindrical waves, which makes it possible to indicate correctly the position of the "focus," to describe approximately (by means of the hyperbolas  $Z^2 - x^2 = \text{const}$  and  $\delta^2 - x^2 = \text{const}$ ) the shapes of the interference fringes, and to present a rather rough general picture of the wave field. The focusing phenomenon, naturally, could not be investigated in this approximation.

## 6. THE WAVES $E_{00}$ , $E_{10}$ , AND $E_{11}$

With the aid of (10) and (11) we can construct the distribution of the wave-field amplitudes in the remaining three beams  $E_{00}$ ,  $E_{10}$ , and  $E_{11}$ . We confine ourselves to presentation of the convolution  $G_{11} * G_{10}$ , which determines the wave field in the beam  $E_{11}$ :

$$G_{11} * G_{10} = \frac{i\chi_1 C}{8} \left[ \frac{Z-x}{Z} J_0 \left( \frac{\chi}{2} \sqrt{Z^2 - x^2} \right) - \frac{\delta-x}{|\delta|} J_0 \left( \frac{\chi}{2} \sqrt{\delta^2 - x^2} \right) \Theta(|\delta| - |x|) \right. \\ \left. - \int_{\max(|x|, |\delta|)}^Z \frac{x}{t^2} J_0 \left( \frac{\chi}{2} \sqrt{t^2 - x^2} \right) dt \right] \exp \left[ -\frac{i\alpha(Z-x)}{4} \right] \Theta(Z - |x|). \quad (22)$$

At  $z_1 = z_2$ , the wave field at the center of the beam has a double peak: at  $|x| \ll Z$  we have

$$G_{11} * G_{10} \approx \frac{i\chi_1 C}{8} \left[ J_0 \left( \frac{\chi Z}{2} \right) - \text{sign}(x) \exp \left( -\frac{\chi|x|}{2} \right) \right] \exp \left[ -\frac{i\alpha}{4}(Z-x) \right]. \quad (23)$$

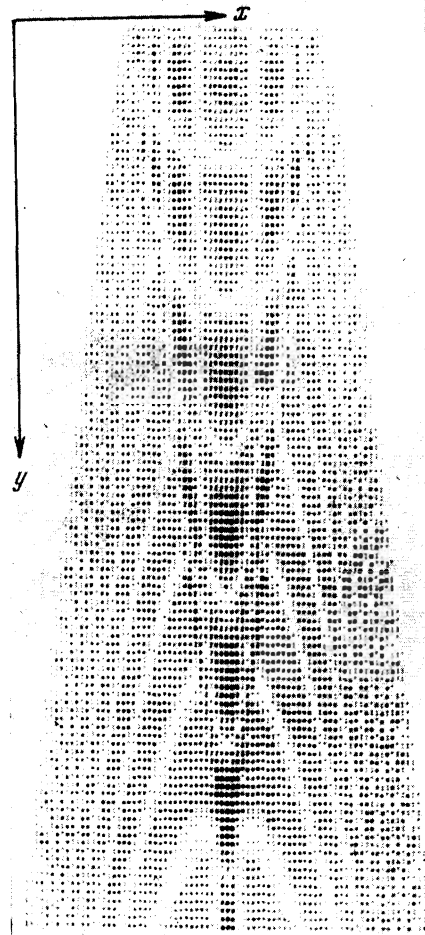


FIG. 4. Computer-calculated slit image past the second plate of the interferometer. The thickness of the second plate is equal to the thickness of the base of the tapered first plate.

The height of this peak, however, is comparable with the level of the total background. In particular, the amplitudes of the oscillations of the wave field at the edges of the beam reaches the value  $i\chi_1 C/4$ .

We note that the beam  $E_{10}$ , if we omit the phase factor  $\exp(i\alpha x/4)$ , is the mirror image of the beam  $E_{11}$  (with  $x$  replaced by  $-x$  and  $\delta$  by  $-\delta$ ). The beam  $E_{00}$  contains the peak (19) with opposite sign, but the principal role is assumed, of course, by the kinematic image of the entrance slit, which is located at the characteristic  $x = Z$  corresponding to the direction of the transmitted wave. By way of illustration, Fig. 5 shows the calculated intensity distribution in the beams  $E_{00}$ ,  $E_{10}$ , and  $E_{11}$  under the same conditions as in Fig. 2<sup>1)</sup>.

## 7. SUPERPOSITION OF BEAMS. IMAGE OF STACKING FAULT AND OF CRACK

The preceding analysis pertained to the case  $d > z_1 + z_2$ , when the distance between the interferometer plates is large enough to permit the beams to become geometrically split. In the opposite case, additional interference of the superimposed beams takes place. An example is the image of a crack. To exclude the contribution of the elastic fields to the crack image, it is advantageous to choose the diffraction vector parallel to the vertex of the crack. The parts of the crystal separated by the crack constitute in this case blocks of an interferometer with wedge-shaped plates and  $d \ll z_1 + z_2$ .

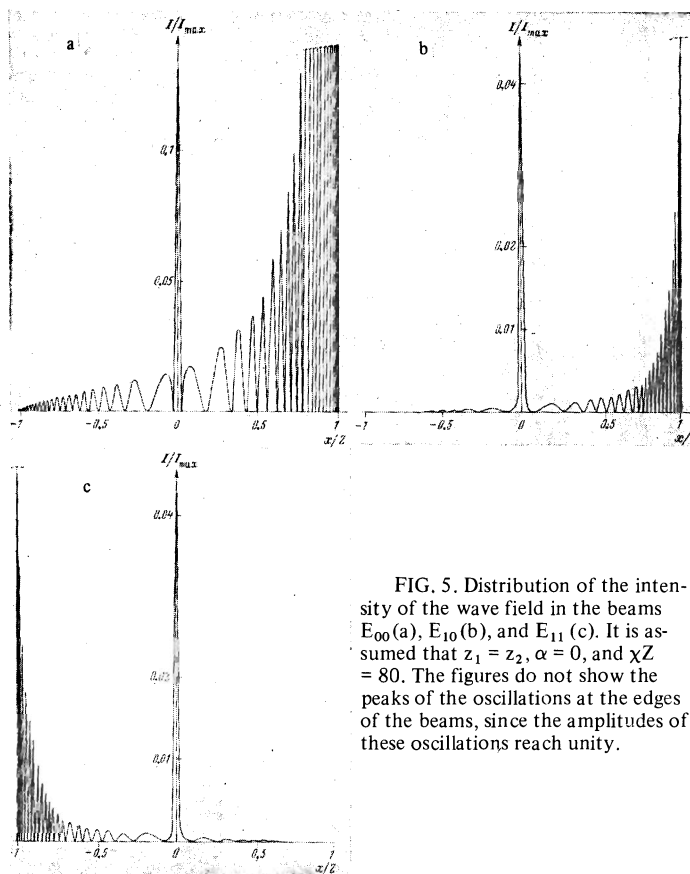


FIG. 5. Distribution of the intensity of the wave field in the beams  $E_{00}$  (a),  $E_{10}$  (b), and  $E_{11}$  (c). It is assumed that  $z_1 = z_2$ ,  $\alpha = 0$ , and  $\chi Z = 80$ . The figures do not show the peaks of the oscillations at the edges of the beams, since the amplitudes of these oscillations reach unity.

Another example may be the problem of the image of a stacking fault parallel to the crystal surface. Here  $d \ll \Lambda$ , but it is necessary to take into account the relative shift of the crystal blocks separated by the stacking fault and constituting the plates of the interferometer. Since the value of this shift does not agree with the translation vector, the phase of the reflected wave acquires

a certain additional shift  $\psi$  relative to the phase of the transmitted wave. As a result, the image of the stacking fault is given by the linear combinations

$$G_{00} * G_{00} + e^{i\psi} G_{01} * G_{10}, \quad G_{10} * G_{00} + e^{i\psi} G_{11} * G_{10}.$$

Focusing of the wave field under stacking fault is again determined by expression (22), which confirms the arguments presented in a number of papers [6], based on analysis of the x-ray paths in the geometrical-optics approximation; these arguments are insufficient to solve the problem of the distribution of the intensity of the wave field near the resultant "focus."

In conclusion, the authors thank Z. G. Pinsker for a discussion, which stimulated the study, and P. A. Bezirganyan for organizing the experiments aimed at verifying the developed theory.

<sup>1</sup>In addition to the convolutions considered above, mention should be made also of the convolutions of the type  $G_{00} * G_{11}$ , which are of considerable interest, and which contain  $\delta$  functions. These convolutions, corresponding to an extremely narrow image (without diffraction broadening) are not realized in the interferometer of the type considered by us.

<sup>1</sup>V. I. Iveronova and G. L. Revkevich, *Teoriya rasseyaniya rentgenovskikh lucheĭ* (Theory of X-ray Scattering), Nauka, 1972.

<sup>2</sup>A. Authier, A. D. Milne, and M. Sauvage, *Phys. Stat. Sol.* **26**, 469 (1968).

<sup>3</sup>M. Hart and A. D. Milne, *Phys. Stat. Sol.* **26**, 185 (1968).

<sup>4</sup>V. L. Indenbom and F. N. Chukhovskii, *Usp. Fiz. Nauk* **107**, 229 (1972) [*Sov. Phys.-Usp.* **15**, 298 (1972)].

<sup>5</sup>H. Friedman, *Adv. in Spectroscopy* **2**, 57 (1964).

<sup>6</sup>N. Kato, K. Usumi, and T. Katagawa, *Adv. X-Ray Anal.* **10**, 46 (1967); A. Authier and M. Sauvage, *J. de Phys.* **27**, C3-237 (1966); A. Authier, *Phys. Stat. Sol.* **27**, 77 (1968).

Translated by J. G. Adashko  
114